

## Pulsed plasma polymerization for controlling shrinkage and surface composition of nanopores

This article has been downloaded from IOPscience. Please scroll down to see the full text article.

2011 Nanotechnology 22 285304

(<http://iopscience.iop.org/0957-4484/22/28/285304>)

View [the table of contents for this issue](#), or go to the [journal homepage](#) for more

Download details:

IP Address: 107.35.123.72

The article was downloaded on 03/06/2011 at 21:26

Please note that [terms and conditions apply](#).

# Pulsed plasma polymerization for controlling shrinkage and surface composition of nanopores

Waseem Asghar<sup>1,2</sup>, Azhar Ilyas<sup>1,2</sup>, Rajendra R Deshmukh<sup>3</sup>,  
Sulak Sumitsawan<sup>4</sup>, Richard B Timmons<sup>3</sup> and Samir M Iqbal<sup>1,2,5,6</sup>

<sup>1</sup> Department of Electrical Engineering, University of Texas at Arlington, TX 76011, USA

<sup>2</sup> Nanotechnology Research and Teaching Facility, University of Texas at Arlington, TX 76019, USA

<sup>3</sup> Department of Chemistry and Biochemistry, University of Texas at Arlington, TX 76019, USA

<sup>4</sup> Department of Civil Engineering, University of Texas at Arlington, TX 76019, USA

<sup>5</sup> Joint Graduate Committee of Bioengineering Program, University of Texas at Arlington and University of Texas Southwestern Medical Center at Dallas, University of Texas at Arlington, TX 76010, USA

E-mail: [smiqbal@uta.edu](mailto:smiqbal@uta.edu)

Received 7 January 2011, in final form 2 May 2011

Published 2 June 2011

Online at [stacks.iop.org/Nano/22/285304](http://stacks.iop.org/Nano/22/285304)

## Abstract

Solid-state nanopores have emerged as sensors for single molecules and these have been employed to examine the biophysical properties of an increasingly large variety of biomolecules. Herein we describe a novel and facile approach to precisely adjust the pore size, while simultaneously controlling the surface chemical composition of the solid-state nanopores. Specifically, nanopores fabricated using standard ion beam technology are shrunk to the requisite molecular dimensions via the deposition of highly conformal pulsed plasma generated thin polymeric films. The plasma treatment process provides accurate control of the pore size as the conformal film deposition depends linearly on the deposition time. Simultaneously, the pore and channel chemical compositions are controlled by appropriate selection of the gaseous monomer and plasma conditions employed in the deposition of the polymer films. The controlled pore shrinkage is characterized with high resolution AFM, and the film chemistry of the plasma generated polymers is analyzed with FTIR and XPS. The stability and practical utility of this new approach is demonstrated by successful single molecule sensing of double-stranded DNA. The process offers a viable new advance in the fabrication of tailored nanopores, in terms of both the pore size and surface composition, for usage in a wide range of emerging applications.

 Online supplementary data available from [stacks.iop.org/Nano/22/285304/mmedia](http://stacks.iop.org/Nano/22/285304/mmedia)

(Some figures in this article are in colour only in the electronic version)

## 1. Introduction

The use of  $\alpha$ -hemolysin protein pores for single and double-stranded DNA translocation have inspired the development of solid-state nanopores for DNA and protein analysis [1–10].

In these studies, the translocation of molecules is monitored using a dual compartment setup, with the compartments separated by a membrane having a single nanopore. An applied potential produces a steady-state ionic current flow from one compartment to the other. For example, the passage of negatively charged DNA molecules through the nanopore provides characteristic current blockage pulses for

<sup>6</sup> Address for correspondence: Department of Electrical Engineering, 500 S Cooper Street #217, Arlington, TX 76019, USA.

each particular analyte. Nanopore biosensors have been used to study various biophysical properties of DNA [11].

Unfortunately, limited analytical capabilities are encountered with respect to the utilization of biological pores. These limitations include restricted variations in experimental conditions, such as the temperature, pH, salinity, range of pore sizes, and mechanical properties [12, 13]. As a result, a great deal of interest has developed in the fabrication of solid-state nanopores for sensing applications. Ideally, the fabrication technique should offer control of the nanopore diameter, channel length and surface composition. Examples of techniques recently employed in the fabrication of these nanopores include focused ion or electron beam sculpting, transmission electron microscope (TEM) induced drilling/shrinking, and feedback chemical etching [14–18]. As documented in these reports, significant progress has been achieved in terms of the fabrication of solid-state nanopores and their applications. Examples of such applications include transducing ligand binding mechanisms into electrochemical signals, DNA charge measurements, and discriminating single base mismatch between target DNA molecules [2, 19–21].

Despite these impressive advances, it has become clear that improved control of both nanopore diameter and pore-wall chemical composition is highly desired. Toward this end, the diameters of solid-state nanopores have been reduced using shrinking or deposition processes. For example, TEM and field emission scanning electron microscope (FESEM) shrinking has been investigated [22, 23]. However, to date, only smaller pores have been shrunk using these approaches. Furthermore, it has been reported that nanopore radii shrink only when the condition  $r < h/2$  is satisfied, where  $r$  and  $h$  are the radius and thickness of the nanopore, respectively, thus introducing an inherent limitation in using these techniques [14]. Atomic layer deposition has also been used to shrink pores but suffers from excessively long deposition times [24]. With respect to chemical composition, it should be noted that the artificial nanopores are fabricated in  $\text{SiO}_2$  or  $\text{Si}_3\text{N}_4$  membranes, thus severely limiting control of the nanopore surface properties.

In light of the above considerations, a single step process that simultaneously provides control of both pore size and surface chemistry is of considerable interest. Herein, we report a rapid solid-state nanopore fabrication and controlled pore shrinking process which does provide simultaneous *in situ* control of surface properties. For this purpose, a pulsed plasma polymer film (PPPF) deposition technique has been employed. As shown in prior pulsed plasma polymerization studies, the chemical composition of the plasma generated polymer films, including cross-link density and surface density of reactive functional groups, can be controlled by simple adjustment of the plasma on to off times during the deposition process [23]. Furthermore, as recently demonstrated, the film thickness control varies linearly with deposition times, and thickness controllability extends to the range of a few nanometers [25, 26]. Most importantly, the pulsed plasma deposited polymeric films exhibit excellent substrate conformability on porous substrates, as recently demonstrated in regulating gas permeation rates through track-etched nanoporous membranes [27].

## 2. Materials and methods

### 2.1. Nanopore fabrication process

The fabrication process was initiated with 300 nm oxidation of double side polished Si wafer followed by photolithography to open square etch-start windows on one side of the wafer. The process continued with wet etching of  $\text{SiO}_2$  with buffered hydrofluoric acid. Silicon was etched through square openings using tetramethylammonium hydroxide (TMAH) anisotropic wet etching at 90 °C and 1:3 (vol:vol) in deionized water. The self-limiting etch stopped once a square window of  $70 \times 70 \mu\text{m}^2$  in  $\text{SiO}_2$  was reached. The thickness of the  $\text{SiO}_2$  membrane was then reduced to 30 nm by reactive ion etching (RIE) using tetrafluoromethane at 100 W and gas flow pressure of 20 sccm. Etch rate of the RIE process was characterized, before etching of membranes, using an ellipsometer. Dry etching of both front and back sides was employed to estimate the membrane thickness after the RIE process. The focused ion beam (FIB, ZEISS 1540XB) was then used to drill small pores of diameter between 100 and 400 nm, using a 30 kV acceleration voltage and gallium ions. Different milling currents (1, 2, 5 and 10 pA) and FIB drilling times (10–30 s) were used to drill pores of the desired diameters.

### 2.2. PPPF deposition

Polymer film deposition was carried out using a home built plasma reactor system, as previously described [25]. The substrates to be coated were located on the center of the base plate of the 6 inch conical reactor. The substrates were subjected initially to a brief 30 s exposure to a pulsed Ar plasma to remove any adsorbed materials. The Ar flow was then terminated and the plasma polymerization of the methacrylic acid (MAA) monomer was initiated. The RF frequency employed for the plasma discharge was 13.56 MHz. The power inputs employed into the reactor were 160 W and 200 W for pulsed and continuous wave plasma respectively. The plasma pulse widths employed were in the millisecond range, with the specific plasma on/off ratio employed for each run set independently. The monomer pressure employed was 160 mTorr for all deposition runs. The MAA (99%, Sigma-Aldrich) was outgassed repeatedly prior to use by freeze drying. Polished Si substrates were employed for the XPS and film deposition rate studies, whereas transparent KBr discs were employed for obtaining the Fourier transform infrared spectroscopy (FTIR) spectra. The  $\text{SiO}_2$  nanopore containing membranes were treated with similar plasma polymerization as described above.

### 2.3. $I$ – $V$ measurement setup

The  $I$ – $V$  measurements were carried out in an aqueous solution of 1 M potassium chloride, using Ag/AgCl electrodes. All measurements were done using an Axon 200B amplifier (Axon Instruments) operated in resistive feedback mode. The head stage and nanopore membrane were placed inside a grounded metallic Faraday cage to reduce the effects of environmental noise. The amplified signal was fed to a

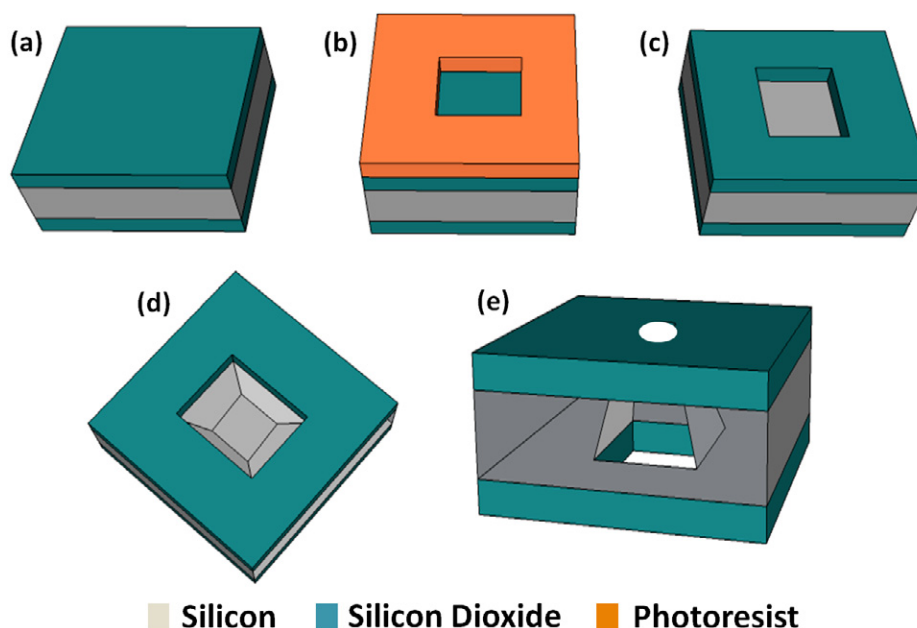


**Figure 1.** Process flow for the fabrication of nanopores using FIB. (a) Oxidized double side polished wafer with 300 nm SiO<sub>2</sub>. (b) Wafer coated with photoresist followed by photolithography to open etch windows in SiO<sub>2</sub>. (c) Wet etch with BHF. (d) TMAH etch to create diaphragm/membranes of 70 × 70 μm<sup>2</sup>. (e) RIE followed by FIB drilling to create pore ready for polymer deposition.

Digidata 1440A data acquisition system (Axon Instruments) controlled with PClamp 2.0 software. *I*–*V* measurements were performed by using a standard two compartment setup where the nanopore die was sandwiched between two Teflon blocks [21]. Polydimethylsiloxane (PDMS) gaskets were used to avoid leakage of KCl during measurements. The PDMS gaskets were made by mixing the base and curing agent at 10:1 ratio in a glass Petri dish. The PDMS mixture was heated to 100 °C for 12 h for polymerization. The solid PDMS was then cut into small gaskets of compatible dimensions.

#### 2.4. DNA translocation through nanopores

The 48.5 kbp double-stranded λ-DNA was used as received. The typical concentration of λ-DNA used in the translocation experiment was 3 nM. The current was allowed to stabilize before the introduction of DNA into the negative bias chamber of the setup [21]. All the translocation experiments were performed at room temperature.

### 3. Results and discussion

The process flow employed in the fabrication of the nanopore membrane is shown in figure 1. Nanopores were drilled in a 30 nm thick SiO<sub>2</sub> membrane as described in section 2. Pulsed plasma polymer was deposited to reduce the diameters of the nanopores and to simultaneously provide carboxylic acid groups on the pore–wall surfaces. The composition of the polymer films was verified using FTIR (figure 2(a)) and XPS (figure 2(b)). As shown in the transmission spectrum of the plasma synthesized polymer film of MAA, a very broad absorption band, extending from approximately 3500 to 2800 cm<sup>−1</sup> is clearly evident in the film. This absorption

band can unequivocally be assigned to –COOH groups, with the unusual broadness of this band reflecting the presence of varying extents of H-bonds from the –OH groups of the –COOH functionality [28]. The other absorption bands, centered around 2900, 1700 and 900 cm<sup>−1</sup>, are attributable to C–H and C=O vibrational modes, expected for a poly-MAA film. High resolution C(1s) XPS spectra, obtained from MAA films plasma polymerized under pulsed and continuous wave (CW) conditions, document the controllability of the MAA film composition as a function of the deposition condition employed. Examples of this controllability are shown in figure 2(b), for films prepared under CW, as compared to pulsed conditions using 1 ms on/5 ms off, and 3 ms on/30 ms off pulse widths. Of particular importance is the high binding energy peak, centered near 289 eV, which can be uniquely assigned to the carboxylic (COO) group [29]. Clearly, as shown in these spectra, the amount of the –COOH groups, relative to the total carbon content, increases significantly as the plasma duty cycle employed in film formation is decreased. This controlled variation in the –COOH surface density was quantified by integration of the deconvoluted C(1s) high resolution photoelectron spectra. Specifically, the per cent contribution of the –COOH groups (289 eV) to the total carbon 1s electrons is as follows: CW: 4.0%; 1 ms on/5 ms off 5.2%; 3 ms on/30 ms off 8.0%. Thus, as these XPS spectra clearly reveal, a substantially higher surface density of –COOH groups is present in the film deposited under pulsed compared to CW conditions, with this percentage increasing further as the plasma duty cycle employed is decreased.

The linear dependence of the MAA film thickness on the deposition time was verified with profilometer measurements (supplementary figure 1 available at [stacks.iop.org/Nano/22/285304/mmedia](http://stacks.iop.org/Nano/22/285304/mmedia)). The linearity of the film deposition rate

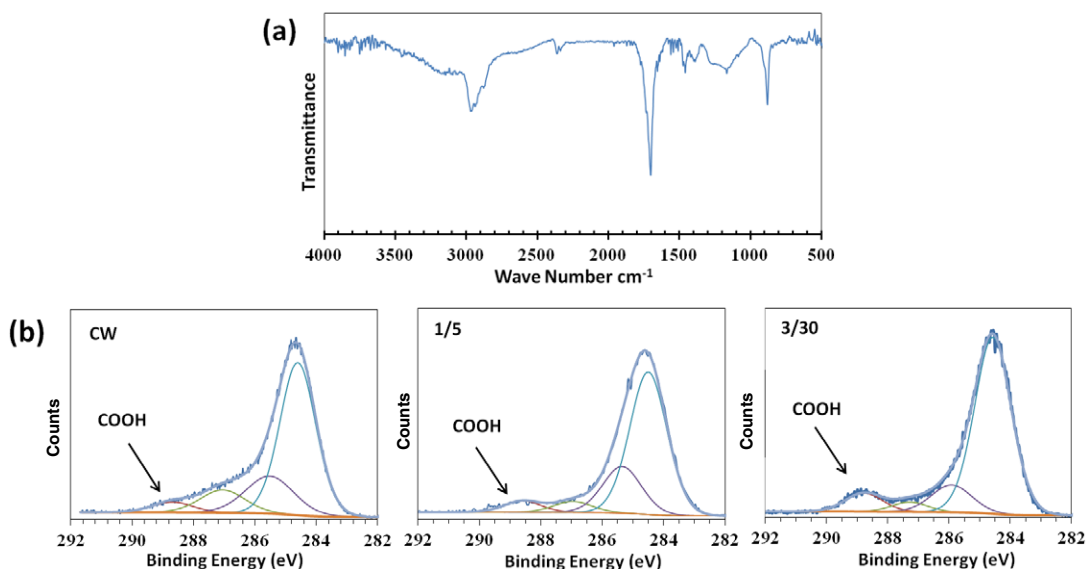


**Figure 2.** Polymer characterization data. (a) FTIR transmission spectrum of plasma polymerized MAA films, deposited using a pulsed plasma of 3 ms on and 30 ms off, 150 W peak power input and 160 mTorr monomer pressure. (b) High resolution C(1s) spectra of polymer films obtained from plasma polymerization of MAA under continuous wave (CW) and pulsed conditions (on/off pulse plasma ratio of 1/5 and 3/30).

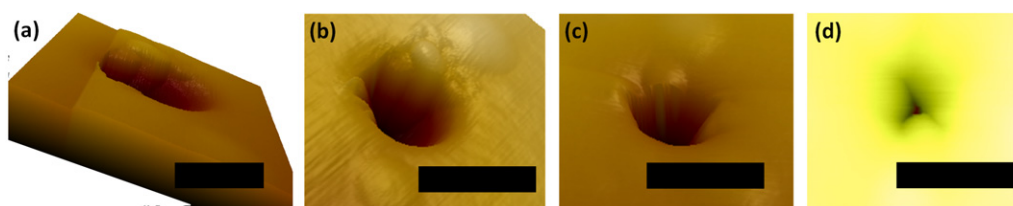


**Figure 3.** AFM micrographs of the nanopore following PPPF deposition. (a) AFM micrograph of the nanopore (300 nm) as fabricated with FIB. (b) AFM micrograph of the nanopore (~190 nm diameter) after 8 min of PPPF deposition. (c) ~120 nm diameter after 13 min of PPPF deposition. (d) ~10 nm diameter after 21 min of PPPF deposition. The AFM data clearly shows that the deposition rate is almost constant at ~14 nm of pore diameter reduction/min. All scale bars are 200 nm.

extended over the entire range of thicknesses examined (from 15 to 170 nm).

The plasma operating conditions were adjusted for a deposition rate of  $\sim 8 \text{ nm min}^{-1}$  using 150 W input power, 160 mTorr monomer pressure and a pulsed plasma duty cycle involving plasma on and off times of 3 ms and 30 ms, respectively. These were the same plasma conditions employed during production of the films for the FTIR, XPS (figure 2) and film thickness measurements (supplementary figure 1 available at [stacks.iop.org/Nano/22/285304/mmedia](http://stacks.iop.org/Nano/22/285304/mmedia)).

A 320 nm pore, fabricated using FIB, was reduced to 80 nm diameter using PPPF deposition, as shown in supplementary figure 2 (available at [stacks.iop.org/Nano/22/285304/mmedia](http://stacks.iop.org/Nano/22/285304/mmedia)). The pore reduction was clearly revealed by the SEM imaging; however the nonconductive nature of the film showed a diffused boundary of the pore geometry. Additionally, the electron beam energy damaged the surface of the nanopore. In fact, the 80 nm nanopore closed during SEM imaging due to surface relaxation of the polymer film. In the case of  $\text{SiO}_2$  membranes, the TEM or FESEM electron beam has been reported to effectively melt even  $\text{SiO}_2$  to flow and adopt the minimum surface energy configuration which

results in pore shrinking [14, 23]. When the nanopore diameter was below 100 nm, the polymer layer closed the nanopore putatively from reorganization of the polymer film, promoted by the electron beam exposure. Alternatively, an atomic force microscope (AFM) was used to characterize and measure the plasma polymer deposition shrinkage of the nanopore, as shown in figure 3. AFM micrographs reveal a very uniform surface morphology of the pore after PPPF deposition, and clearly illustrate the excellent control on the pore shrinkage provided by the pulsed plasma deposition approach. A 300 nm pore was reduced to 10 nm with PPPF deposition in a sequence of three stepwise reductions involving deposition times of 8, 13 and 21 min. It is evident from the AFM micrograph data that the particular plasma process produced a uniform diameter reduction rate of  $\sim 14 \text{ nm min}^{-1}$ . This shrinkage rate is in good agreement with the film deposition rates shown in supplementary figure 1 (available at [stacks.iop.org/Nano/22/285304/mmedia](http://stacks.iop.org/Nano/22/285304/mmedia)) in that the pore shrinkage rate is twice that of the film deposition rate on a flat substrate.

To electrically characterize the nanopore shrinkage, current–voltage ( $I$ – $V$ ) measurements were carried out in an ionic solution of 1 M potassium chloride (KCl). The  $I$ – $V$

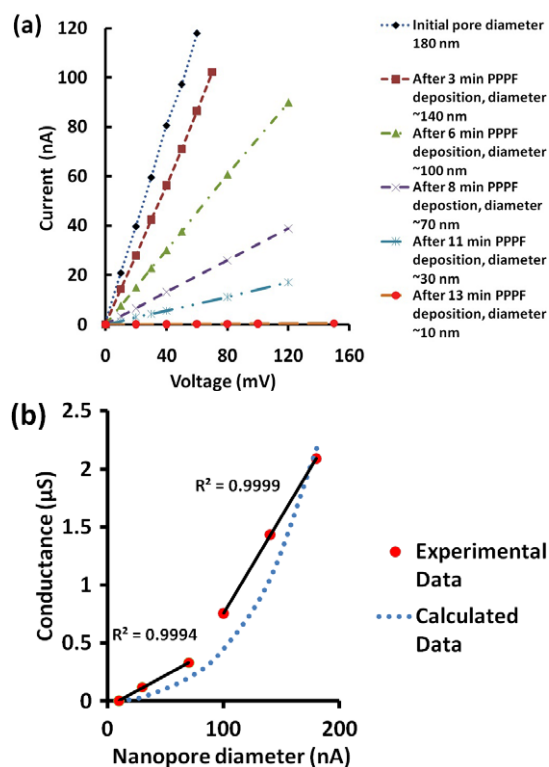


**Figure 4.**  $I$ – $V$  measurements during polymer deposition. (a) Shows the scaling of the current with the PPPF deposition. The initial nanopore diameter was 180 nm as fabricated with FIB. The pore diameter reduced to 140, 100, 70, 30 and 10 nm after 3, 6, 8, 11 and 13 min of polymer deposition respectively. The  $I$ – $V$  data shows linear behavior over the whole range of nanopore diameters. (b) Shows the conductance plot for different nanopore diameters. The calculations are for 10 mV of applied potential and 1 M KCl concentration (blue dotted line). The measured data (red large dots) shows a good fit to the model curve. The two regimes of the fit line stem from the conical geometry of the nanopore (explained in text). One linear region is before and one after 100 nm pore diameter.

measurements were performed after each PPPF deposition step. The electrical data confirmed that the pore remained open after each plasma treatment step and, more importantly, a progressive decrease in conductance was observed with increasing plasma deposition times. Thus these  $I$ – $V$  measurements depict a sequential decrease in pore diameter with increasing polymer film thickness. For each pore diameter examined, the current varied linearly with the applied voltage (figure 4(a)).

Conductance of the nanopore,  $G$ , was also measured at 1 M electrolyte concentration. In previous reports, different models have been proposed to fit  $G$  of nanopores [23, 30, 31]. Bulk charge carriers were expected to dominate the ion flow at 1 M KCl. The surface charge effect was also neglected in these models at higher salt concentrations. For our  $G$  data fit, we considered a purely cylindrical nanopore channel as proposed by Smeets *et al* [31]. Based on the uniform plasma deposition rate and the AFM data, a simple resistance equation,  $G = \sigma\pi r^2/L$ , can be used to model the behavior of the nanopore, where  $\sigma$  is the conductivity of KCl solution,  $L$  is the channel length and  $r$  is the radius of the nanopore. Our data reveal two regimes for conductance that can be fit to

this model, as shown in figure 4(b). Basically, a non-linear variation in  $G$  is observed with the sequential variation in pore diameter. This can be reasonably explained in terms of a non-linear plasma polymer deposition through the whole channel length of the pore. A more localized nanopore surface edge deposition, compared to that on inside vertical walls may well have occurred, particularly as the pore shrank and the hole aspect ratio increased. The overall pore geometry would thus have been deviated from a perfectly cylindrical geometry as the plasma polymer film thickness increased. The deposition rate on the pore–wall would also vary along the length of the nanopore channel due to reduced diffusion of polymer vapors during the deposition process. Additionally, the upstream volume transport of pre-polymer gaseous species through the nanopore causes a drop in pressure. These effects can be accommodated by changing  $r^2$  to  $r \times r^*$ , where  $r$  and  $r^*$  would be the top and bottom radii of the nanopore respectively [30]. In fact, the above observations are in line with gas transport phenomena through the membranes as reported before [32]. This pressure drop across the membrane can be described as an exponential function of time  $t$ , as shown by equation (1) [32]:

$$\Delta p(t) \approx p_0 e^{-\epsilon A D_k / V_u l^2 t}. \quad (1)$$

Here  $\Delta p(t)$  is the pressure drop across the membrane as a function of time  $t$ ,  $p_0$  is the pressure drop at time  $t = 0$ ,  $\epsilon$  is the porosity of the membrane,  $A$  is the exposed area,  $D_k$  is Knudsen diffusivity,  $V_u$  is the volume upstream of the membrane,  $l$  is the length of the nanopore channel and  $t$  is the time.

In order to examine the PPPF nanopore current behavior at different salt concentrations, we used 0.1 and 1 M KCl for  $I$ – $V$  measurements with a 10 nm PPPF nanopore (figure 5(a)). The nanopore showed linear current behavior. At high KCl concentrations ( $[KCl] \geq 100$  mM), the conductivity of the nanopore showed a linear dependence on the voltage as expected for the bulk conductivity of KCl during the voltage sweep [16, 31]. Theory predicts that when the diameter of the nanopore is comparable to the diameter of the diffusing ionic species (0.3 nm), the diffusion of the species would be reduced due to hindered diffusion which would reduce the conductivity of the nanopore as compared to bulk conductivity [33, 34]. It was also reported that decreased electrostatic interactions in nanopores would reversely increase the nanopore conductivity when compared to bulk conductivity [35]. MAA polymer film has  $\text{COO}^-$  fixed charges at pH 7.0 which would have an incremental effect on the concentration of  $\text{K}^+$  ions inside the channel due to the electrical double layer at the walls of the nanopore [36]. However, the electrostatic enhancement would be compensated by the hindered diffusion effect [33]. So the conductivities of KCl in the nanopore and bulk solution can be considered approximately equal. Conical nanopores in track-etched poly(ethylene terephthalate) (PET) membranes had been reported to rectify the ionic current due to entrapment of the charges because of the electrical double layer [36]. Our nanopore is also conical but, interestingly, it did not show rectified current behavior. PET membranes are generally very thick (10–12  $\mu\text{m}$ ) as compared to our polymer nanopore thickness ( $\sim 200$  nm) [37]. So the nanochannels fabricated in

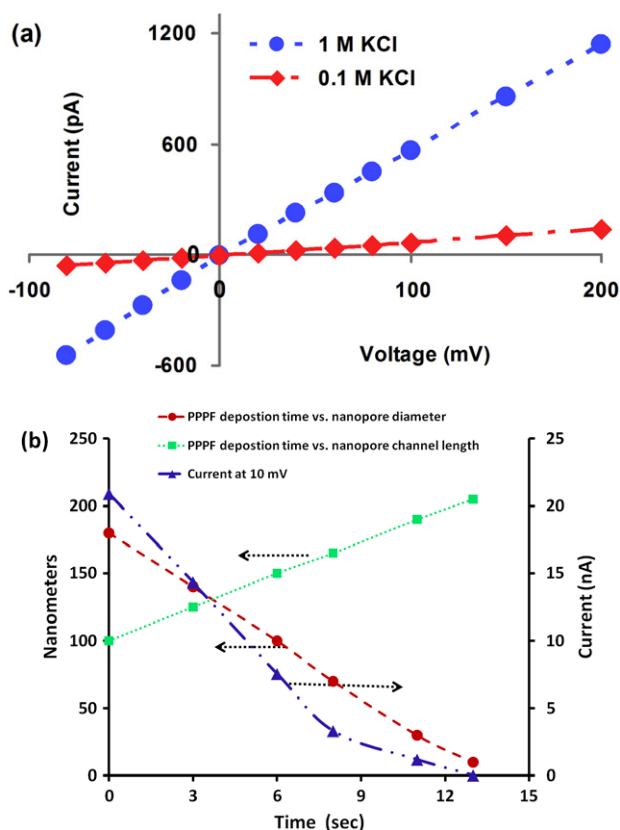


**Figure 5.** Pore  $I$ - $V$  characterization at different salt concentrations and overall process analysis (a) PPPF deposited 10 nm nanopore was measured for  $I$ - $V$  analysis at salt concentrations of 0.1 M (diamonds) and 1 M (circles). The current scaled linearly with the voltage at both of the salt concentrations. (b) The plots show the nanopore diameter (dots) and channel length (squares) with respect to PPPF deposition time. The linear behavior of the channel length and diameter shows the uniform deposition rate for the whole process under optimal applied input power and process pressure. The initial pore diameter and channel length were 180 nm and 100 nm respectively. After approximately 4 min of deposition the channel length and diameter became equal in dimension. The measured current (triangles) also scaled almost linearly with the nanopore diameter which again showed a uniform deposition rate with time.

PET membranes made perfect conical structures of channels of length 12  $\mu\text{m}$  having a 300 nm opening at one side and a 5–10 nm opening at the other side of the membrane. Our polymer nanopore would not be perfectly conical in view of the thinness of the membrane and conformal nature of the plasma polymer MAA film. We propose that this type of nanopore would not rectify the current signal because there would not be significant asymmetry in the electrostatic potential along the channel during the voltage sweep [37].

The overall pore shrinkage data are plotted in figure 5(b). The plot is based on the AFM micrographs, the profilometer and ionic current data. The pore diameter and channel length showed linear behavior when plotted against time. The ionic current showed two regimes of linearity as explained before in the text.

To demonstrate the viability of polymer deposited nanopores for single molecule biosensor applications, translocation experiments using DNA were carried out. For this

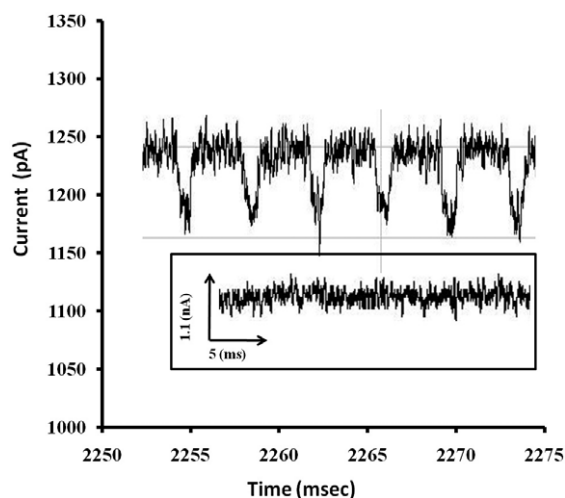


**Figure 6.** DNA translocation through the nanopore. Typical current blockades were seen when  $\lambda$ -DNA at 3 nM concentration was added to the negative bias compartment at 1 M KCl and 100 mV applied potential. The inset shows the baseline current before the introduction of  $\lambda$ -DNA.

purpose, unmethylated 48.5 kbp double-stranded  $\lambda$ -DNA (Promega, Benelux) in 1 M KCl buffered with 10 mM Tris-HCl and 1 mM EDTA solutions at pH 7.5 was used with the 10 nm pore. The translocation data was recorded using a 100 mV applied potential. Open pore  $I$ - $V$  measurements were conducted before the introduction of the  $\lambda$ -DNA into the negative-biased compartment of the cell (inset of figure 6). The translocation of the DNA resulted in current blockages as shown in figure 6. The current signal was digitized at 200 kHz with a low pass filter at a cutoff frequency of 10 kHz. The average translocation time for one  $\lambda$ -DNA was approximately 2.2 ms which was in good agreement with previous reports [31]. After the DNA was added, many transient current blockage pulses were observed. The nanopore diameter was also calculated from the magnitude of current blockage pulses using the relation  $\Delta I/I_{\text{open}} = A_{\text{DNA}}/A_{\text{nanopore}}$ , where  $\Delta I \sim 65$  pA was the current blockage magnitude from DNA translocation,  $I_{\text{open}} \sim 1240$  pA was open pore current,  $A_{\text{DNA}} \sim 5$  nm<sup>2</sup> was the average cross-sectional area of the double strand DNA and  $A_{\text{nanopore}}$  was the nanopore diameter [38, 39]. The value of  $A_{\text{nanopore}}$  was calculated to be equal to 95.38 nm<sup>2</sup>. Assuming a circular pore, the diameter of the nanopore was found to be equal to 11 nm which was in good agreement with the nanopore diameter measured with AFM.

#### 4. Conclusions

The utility of employing a pulsed plasma polymerization process to reduce nanopore diameters, in a highly controlled fashion, for use in nanopore sensing applications has been demonstrated for the first time. In contrast with other studies, the pore shrinkage process involves only a single step and provides excellent control of the pore diameter. The control of pore shrinkage has been characterized microscopically with AFM and a variety of conductivity measurements. The viability of this approach for single molecule sensor applications has been demonstrated using double-stranded

DNA. The reported novel method permits accurate control of both pore diameter as well as molecular tailoring of the surface chemistry of the pores. The latter can be accomplished simply by the appropriate choice of monomer and/or by attachment of the appropriate molecules to reactive functional groups retained in the polymer films.

## Acknowledgments

We acknowledge useful discussions with Hung Chang and Yuan Wan, and thank Joseph A Billo for help in data analysis. We thank the staff at the Nanotechnology Research and Teaching Facility for help in fabrication and are grateful to Jiechao Jiang (UTA Characterization Center for Materials and Biology—C<sup>2</sup>MB) for help with chip characterization. The work was supported by grants from The Metroplex Research Consortium for Electronic Devices and Materials (MRCEDM), Arlington, Texas and National Science Foundation CAREER grant number ECCS-0845669. Waseem Asghar and Azhar Ilyas were partially supported by a fellowship from the Consortium for Nanomaterials for Aerospace Commerce and Technology (CONTACT) program, Rice University, Houston, TX, USA.

## References

- [1] Gyurcsányi R E, Vigassy T and Pretsch E 2003 Biorecognition-modulated ion fluxes through functionalized gold nanotubes as a novel label-free biosensing approach *Chem. Commun.* **2003** 2560–1
- [2] Chang H, Venkatesan B M, Iqbal S M, Andreadakis G, Kosari F, Vasmatzis G, Peroulis D and Bashir R 2006 DNA counterion current and saturation examined by a MEMS-based solid state nanopore sensor *Biomed. Microdevices* **8** 263–9
- [3] Siwy Z, Trofin L, Kohli P, Baker L A, Trautmann C and Martin C R 2005 Protein biosensors based on biofunctionalized conical gold nanotubes *J. Am. Chem. Soc.* **127** 5000
- [4] Mathé J, Aksimentiev A, Nelson D R, Schulten K and Meller A 2005 Orientation discrimination of single-stranded DNA inside the-hemolysin membrane channel *Proc. Natl Acad. Sci.* **102** 12377
- [5] Kasianowicz J J, Brandin E, Branton D and Deamer D W 1996 Characterization of individual polynucleotide molecules using a membrane channel *Proc. Natl Acad. Sci.* **93** 13770
- [6] Gu L Q, Cheley S and Bayley H 2001 Capture of a single molecule in a nanocavity *Science* **291** 636
- [7] Muthukumar M and Kong C Y 2006 Simulation of polymer translocation through protein channels *Proc. Natl Acad. Sci.* **103** 5273
- [8] Ramachandran A, Liu Y, Asghar W and Iqbal S M 2009 Characterization of DNA-nanopore interactions by molecular dynamics *Am. J. Biomed. Sci.* **1** 344–51
- [9] Zelzer M and Alexander M R 2010 Nanopores in single- and double-layer plasma polymers used for cell guidance in water and protein containing buffer solutions *J. Phys. Chem. B* **114** 569–76
- [10] Venkatesan B M, Shah A B, Zuo J-M and Bashir R 2010 DNA sensing using nanocrystalline surface-enhanced Al<sub>2</sub>O<sub>3</sub> nanopore sensors *Adv. Funct. Mater.* **20** 1266–75
- [11] Heng J B, Aksimentiev A, Ho C, Marks P, Grinkova Y V, Sligar S, Schulten K and Timp G 2005 Stretching DNA using the electric field in a synthetic nanopore *Nano Lett.* **5** 1883
- [12] DeGuzman V S, Lee C C, Deamer D W and Vercoutere W A 2006 Sequence-dependent gating of an ion channel by DNA hairpin molecules *Nucleic Acids Res.* **34** 6425–37
- [13] Bockelmann U and Viasnoff V 2008 Theoretical study of sequence-dependent nanopore unzipping of DNA *Biophys. J.* **94** 2716–24
- [14] Storm A J, Chen J H, Ling X S, Zandbergen H W and Dekker C 2003 Fabrication of solid-state nanopores with single-nanometre precision *Nat. Mater.* **2** 537–40
- [15] Chang H, Iqbal S M, Stach E A, King A H, Zaluzec N J and Bashir R 2006 Fabrication and characterization of solid-state nanopores using a field emission scanning electron microscope *Appl. Phys. Lett.* **88** 103109
- [16] Venkatesan B M, Dorvel B, Yemencioğlu S, Watkins N, Petrov I and Bashir R 2009 Highly sensitive, mechanically stable nanopore sensors for DNA analysis *Adv. Mater.* **21** 2771
- [17] Park S R, Peng H and Ling X S 2007 Fabrication of nanopores in silicon chips using feedback chemical etching *Small* **3** 116
- [18] Schneider G F, Kowalczyk S W, Calado V E, Pandraud G, Zandbergen H W, Vandersypen L M K and Dekker C 2010 DNA translocation through graphene nanopores *Nano Lett.* **10** 3163–7
- [19] Chang H, Kosari F, Andreadakis G, Alam M A, Vasmatzis G and Bashir R 2004 DNA-mediated fluctuations in ionic current through silicon oxide nanopore channels *Nano Lett.* **4** 1551–6
- [20] Benson D E, Conrad D W, de Lorimier R M, Trammell S A and Hellinga H W 2001 Design of bioelectronic interfaces by exploiting hinge-bending motions in proteins *Science* **293** 1641
- [21] Iqbal S M, Akin D and Bashir R 2007 Solid-state nanopore channels with DNA selectivity *Nat. Nanotechnol.* **2** 243–8
- [22] Kim M J, Wanunu M, Bell D C and Meller A 2006 Rapid fabrication of uniformly sized nanopores and nanopore arrays for parallel DNA analysis *Adv. Mater.* **18** 3149–53
- [23] Kim M J, McNally B, Murata K and Meller A 2007 Characteristics of solid-state nanometre pores fabricated using a transmission electron microscope *Nanotechnology* **18** 205302
- [24] Chen P, Mitsui T, Farmer D B, Golovchenko J, Gordon R G and Branton D 2004 Atomic layer deposition to fine-tune the surface properties and diameters of fabricated nanopores *Nano Lett.* **4** 1333–7
- [25] Bhattacharyya D, Pillai K, Chyan O M R, Tang L and Timmons R B 2007 A new class of thin film hydrogels produced by plasma polymerization *Chem. Mater.* **19** 2222–8
- [26] Bhattacharyya D, Yoon W J, Berger P R and Timmons R B 2008 Plasma polymerized multistacked organic bipolar films: a new approach to flexible high dielectrics *Adv. Mater.* **20** 2383–8
- [27] Chapman C L, Bhattacharyya D, Eberhart R C, Timmons R B and Chuong C J 2008 Plasma polymer thin film depositions to regulate gas permeability through nanoporous track etched membranes *J. Membr. Sci.* **318** 137–44
- [28] Socrates G 1994 *Infrared Characteristic Group Frequencies* (New York: Wiley)
- [29] Beamson G and Briggs D 1992 *High Resolution XPS of Organic Polymers: The Scienta ESCA300 Database* (New York: Wiley)
- [30] Nilsson J, Lee J R I, Ratto T V and Letant S E 2006 Localized functionalization of single nanopores *Adv. Mater.* **18** 427–31
- [31] Smeets R M M, Keyser U F, Krapf D, Wu M Y, Dekker N H and Dekker C 2006 Salt dependence of ion transport and DNA translocation through solid-state nanopores *Nano Lett.* **6** 89–95

- [32] Roy S, Raju R, Chuang H F, Cruden B A and Meyyappan M 2003 Modeling gas flow through microchannels and nanopores *J. Appl. Phys.* **93** 4870
- [33] Harrell C C, Lee S B and Martin C R 2003 Synthetic single-nanopore and nanotube membranes *Anal. Chem.* **75** 6861–7
- [34] Deen W M 1987 Hindered transport of large molecules in liquid filled pores *AIChE J.* **33** 1409–25
- [35] Tang Y W, Szalai I and Chan K Y U 2001 Diffusivity and conductivity of a primitive model electrolyte in a nanopore *Mol. Phys.* **99** 309–14
- [36] Siwy Z, Kosińska I D, Fuliński A and Martin C R 2005 Asymmetric diffusion through synthetic nanopores *Phys. Rev. Lett.* **94** 48102
- [37] Siwy Z, Heins E, Harrell C C, Kohli P and Martin C R 2004 Conical-nanotube ion-current rectifiers: the role of surface charge *J. Am. Chem. Soc.* **126** 10850–1
- [38] Saleh O A and Sohn L L 2003 An artificial nanopore for molecular sensing *Nano Lett.* **3** 37–8
- [39] Wu S, Park S R and Ling X S 2006 Lithography-free formation of nanopores in plastic membranes using laser heating *Nano Lett.* **6** 2571–6